

# Enhanced Ultraviolet Spontaneous and Lasing Emission Through Interface Engineering of Patterned Vertically Aligned ZnO Nanowires

Zhen Guo,\* Dongxu Zhao, Lin Li, Caroline Andreazza-Vignolle, Pascal Andreazza, Ligong Zhang, Wei Zhang, and Lianqun Zhou\*

Due to optical radiation losses, a high pumping threshold or low temperature is necessary for driving ultraviolet (UV) light emission devices, and surface/interface engineering method is one of the alternatives for tailoring photon behavior. Here, a fully integrated nanowire (NW) laser device is thus constructed, resulting in suppressed interface light loss. Enhanced UV spontaneous and lasing emission is observed due to adequate gain to compensate for the optical loss. Applying well-aligned ZnO NW cavities, optimized UV spontaneous and lasing emission is realized, supporting an effective optical path through interface engineering for photon extraction. As proven by experimental results, through interface integration with Pt metal for ZnO NWs, 170% photoluminescence (PL) emission enhancement accompanied by 145% broaden emission spectra width in the UV region is obtained. It is also observed that more lasing modes appear when excitation density is high enough, lasing modes interspacing of around 3 nm, and full width at half maximum of the modes  $<0.003$  eV for the lasing device could be observed. The detailed optical simulation is proposed to understand the physical origin of internal mechanisms contributing to the optimized spontaneous and stimulated lasing emission behaviors.

MEMS or NEMS sensors.<sup>[1–8]</sup> Among the most studied nanomaterials, 1D nanowires (NWs) with ultra-high intrinsic photoelectric gain, multiple array light confinement, and subwavelength size effects could be suitable for designing structures with advanced performance, which fully satisfy the practical needs.<sup>[9–12]</sup> Due to the small size and self-formed cavity, semiconductor NWs have attracted more and more attention to fabricating nanostructured lasers,<sup>[13]</sup> which could provide natural cavities for low size lasers.<sup>[15–18]</sup> Among all the low dimensional materials, ZnO is considered to be a promising candidate as a UV media considering its wide bandgap (3.37 eV) and large exciton binding energy of 60 meV, which is suitable for fabricating room temperature optoelectronic devices.<sup>[19–21]</sup> Compared with GaN (25 meV), the large exciton binding energy of ZnO material enables to achieve room temperature optoelectronic devices with high stability.


## 1. Introduction

UV light source such as LEDs and lasers plays an important role in industry, military, and even daily life, which opens a door to obtaining all-optical chips, huge data storages, optical communications, biomedical applications, and highly integrated

At present, optically pumped UV lasing action in ZnO was realized as the gain medium with single forms such as microwires, microspheres, nanoribbons, nanowires, etc.<sup>[22–25]</sup> and the preparation methods could be thermal oxidation, chemical vapor deposition (CVD), hydrothermal reaction, magnetron sputtering, atomic layer deposition (ALD), pulsed laser

Z. Guo, W. Zhang, L. Zhou  
CAS Key Lab of Bio-Medical Diagnostics  
Suzhou Institute of Biomedical Engineering and Technology  
Chinese Academy of Sciences  
No.88, Keling Road, Suzhou 215163, P. R. China  
E-mail: happygzh2000@163.com; zhoulq@sibet.ac.cn  
D. Zhao, L. Zhang  
The State Key Laboratory of Luminescence and Applications  
Changchun Institute of Optics  
Fine Mechanics and Physics  
Chinese Academy of Sciences  
3888 East Nan-Hu Road, Open Economic Zone, Changchun 130033,  
P. R. China

L. Li  
Key Laboratory for Photonic and Electronic Bandgap Materials  
Ministry of Education  
School of Physics and Electronic Engineering  
Harbin Normal University  
Harbin 150025, P. R. China  
C. Andreazza-Vignolle, P. Andreazza  
Centre de Recherche sur la Matière Divisée  
CRMD  
UMR 6619 Université d'Orléans  
CNRS  
1b rue de la ferronnerie, Orléans Cedex 2 45071, France

 The ORCID identification number(s) for the author(s) of this article can be found under <https://doi.org/10.1002/admi.202200024>.

DOI: 10.1002/admi.202200024

deposition (PLD), and so on.<sup>[26,27]</sup> As one alternative method, vertically aligned 002 ZnO NWs applying hydrothermal solution could be fabricated on a large scale with good repeatability, which is beneficial for mass preparation. The optical cavity could be formed through self-assembly owning high crystal quality and ZnO NW lasers are usually observed with end facets serving as Fabry–Pérot (F-P) cavity mirrors, the interface quality of which is much more significant for forming sufficient gain to lasing.<sup>[28,29]</sup> However, due to optical radiation loss, a high threshold is usually required to compensate for light loss for the ZnO lasers due to inner and interface optical loss.<sup>[30,31]</sup>

It is known that light behaviors tailoring could be realized through device structure design, in which light-matter interaction can be greatly modified by surrounding media through surface/interface engineering.<sup>[32,33]</sup> At present, more and more studies on multiple scattering phenomena in micro-/nano-materials have been devoted to exploring mechanisms of cavity quantum electrodynamics, renewable energy, lasing, and imaging fields.<sup>[34,35]</sup> Through micro-/nano-material structure modifications, light transport behavior could be well-modulated to excite a specific part of the active photonic media, and the light emission properties could be well constructed to improve output performance.<sup>[36–38]</sup> Through surface/interface engineering, it is believed that ZnO NW emission devices could be optimized through light-matter interaction modulation for tailoring the optical process.<sup>[33,39–41]</sup>

Here, light confinement modulation was realized based on ZnO NWs through interface engineering end facets through introducing Pt metal, optimized UV spontaneous and lasing emission was realized, supporting an effective optical path through interface engineering for photon extraction, thus a larger internal gain was realized for enhanced spontaneous and lasing emissions. As proven by experimental results, through interface integration with Pt metal for ZnO NWs, 170%

photoluminescence (PL) emission enhancement accompanied by 145% broaden emission spectra width (FWHM) in the UV region was obtained. And laser threshold was further lowered to 7.69 times smaller than that for the ZnO NWs without Pt modification. Strong light confinement was thus realized when the Q factor becomes high enough. Corresponding theory simulation is also proposed to understand the physical origin of UV spontaneous and lasing emission enhancement in ZnO NWs.

## 2. Results and Discussion

### 2.1. Structure Design of Ultraviolet Emission Devices Based on ZnO NW

To construct a low-loss UV NW laser device, cavity quality, and laser facets are two mainly considered factors. As shown in **Figure 1a**, a schematic diagram of a 1D laser device consisting of 002 oriented epitaxial grown ZnO NW assisted with homogeneity film for forming a close contact with the substrate, Pt metal is selected as NW interface engineering material meanwhile as low mismatch material supporting high-quality ZnO semiconductor synthesis to reduce optical loss in the UV region. Compared with conventional mirror end facet structure, and self-assembled NW with close contact structure, a fully integrated NW laser device of semiconductor material with cavity facet interface engineering was thus constructed, resulting in suppressed interface scattering loss, which could be an optimized channel for photonic emission improvement, supporting effective photon interface interaction for optical amplification, thus to obtain larger internal gain for lasing emission. Simulated cross-sectional electric field distribution images of ZnO NW/thin-film/Si and ZnO NW/thin-film/Pt are shown in **Figure 1b,c**, respectively. For the first device structure, the

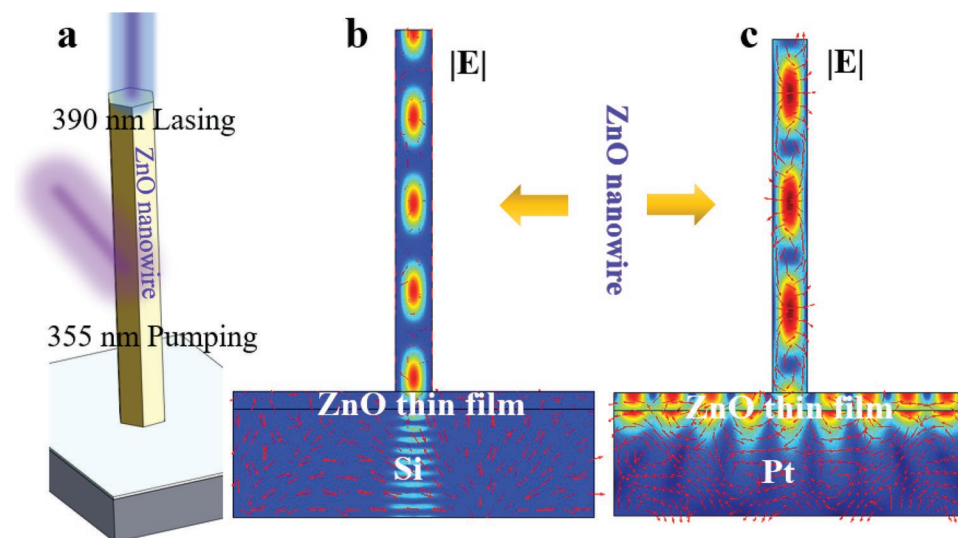


**Figure 1.** Ultraviolet ZnO NW photonic light emission device. a) Schematic diagram of ZnO NW semiconductor lasing device, ZnO NW with hexagonal cross-section is epitaxial grown on ZnO thin film layer assisted with Si or Pt metal. A focused 355 nm ultraviolet femtosecond laser source is applied to pump the ZnO NW. The ZnO photoluminescence waveguides through F-P cavity resonance to produce photonic mode when hybridize with Si or Pt film. b,c) Absolute electric field distribution in ZnO NW supported with Si/ZnO thin film and Pt/ZnO thin film calculated with a finite element method, red arrows indicate the corresponding magnetic field direction. The  $|E|$  as shown in (c) confirms that optical energy interaction with the Pt layer for enhancing spontaneous and stimulated lasing emission.



electromagnetic energy is diffused into the Si substrate region, demonstrating large optical loss. Through applying Pt metal, the efficient light confinement resulted in enhanced optical emission, which owns a larger internal gain by reducing optical loss to the substrate in this configuration, supporting effective spontaneous and lasing emissions based on ZnO NWs.

## 2.2. Structure Characterization of Patterned Vertically Aligned ZnO NWs

As shown in **Figure 2a–c**, top-view scanning electron microscopy (SEM) images of patterned vertically aligned ZnO NWs could be obtained via UV photolithography and hydrothermal

solution process methods. Patterned ZnO NWs could be selectively grown in the place where a thin film of ZnO seed layer is exposed outside, and the ZnO NWs could be prepared in a defined area with density of  $\approx 50$  unit NWs  $\mu\text{m}^{-2}$  by solution process with well 002 orientation, which is suitable for constructing UV light emission devices. Here, the low lattice mismatch ( $\approx 1.4\%$  between c-ZnO and the Pt (111) surface) between Pt metal and ZnO layer is formed, which gives a good growth environment supporting ZnO material alignment orientation, and cross-sectional SEM images showed the obtained ZnO NWs are about  $3\ \mu\text{m}$  in length (**Figure 2d**). The X-ray diffraction (XRD) pattern of the NWs on Pt (thickness:  $300\ \text{nm}$ , **Figure 2e**)/Si substrate is displayed in **Figure 2f**, the diffraction peaks of the sample can be indexed to wurtzite hexagonal ZnO and cubic

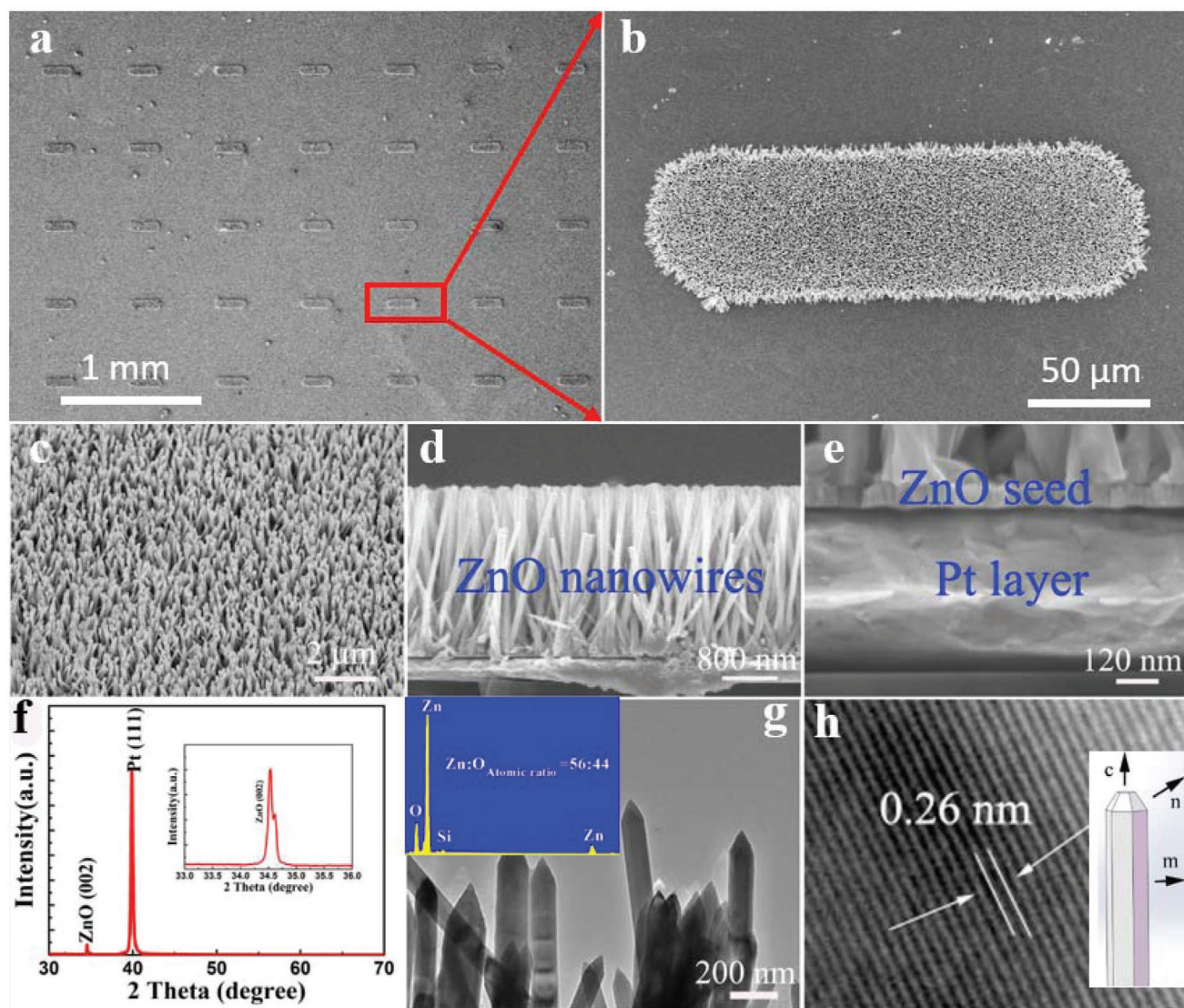


**Figure 2.** Morphology and structural characterization of patterned ZnO NWs. a) Top view SEM image of patterned ZnO NWs on a large scale, b) SEM image of single cluster ZnO NWs, c) amplified SEM image of single cluster ZnO NWs, d,e) cross-sectional SEM images of ZnO NWs and interface image of ZnO NWs/thin-film/Pt, f) XRD 2θ scan of vertically aligned ZnO NWs supporting with Pt layer, g) TEM image shows NWs with sharp tops, and insert shows EDX analysis of ZnO NW with element ratio of Zn: O = 56:44, h) HRTEM image of ZnO NWs, the insert shows a schematic diagram of single ZnO NW.

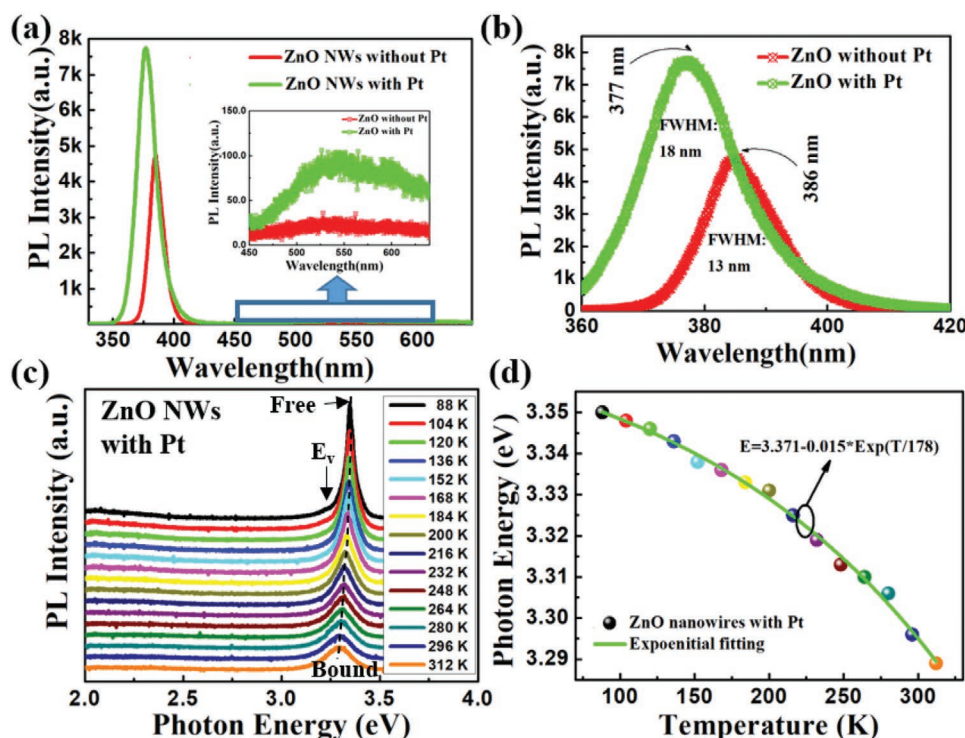


**Figure 3.** Photoluminescence (PL) characterization of ZnO NWs with and without Pt metal. a) Room-temperature PL spectra (from 330 to 650 nm) of ZnO NWs with and without Pt metal, b) PL spectra (from 360 to 420 nm) of ZnO NWs with and without Pt for FWHM comparison, c) temperature-dependent PL spectra of ZnO NWs with Pt from 88 to 312 K, d) photon energy fitting analysis versus temperature for ZnO NWs with Pt as shown in (c).

Pt. For the ZnO NWs, only a (002) diffractive peak could be observed, which indicates c-axis orientation. The peak position for the ZnO NWs is located at  $34.5^\circ$ , which agrees well with the bulk ZnO. The FWHM of the ZnO diffractive peak is  $0.10^\circ$  and the magnified (002) diffraction pattern shown in the insert is comprised of two peaks originating from the diffractions of  $\text{Cu } \alpha_1$  and  $\alpha_2$ , which implies good crystallinity of the ZnO NWs. The transmission electron microscopy (TEM) image of the NWs exhibits a nanoneedle-like shape with a diameter of  $\approx 100$  nm on average (Figure 2g). The high-resolution TEM (HRTEM) image (Figure 2h) shows single-crystal NW grown along the [002] direction with lattice fringes perpendicular to the c-axis, and the equal interplanar distance along the NW was  $2.60\text{ \AA}$ .

### 2.3. Photoluminescence Characterization of ZnO NWs with and without Pt Metal

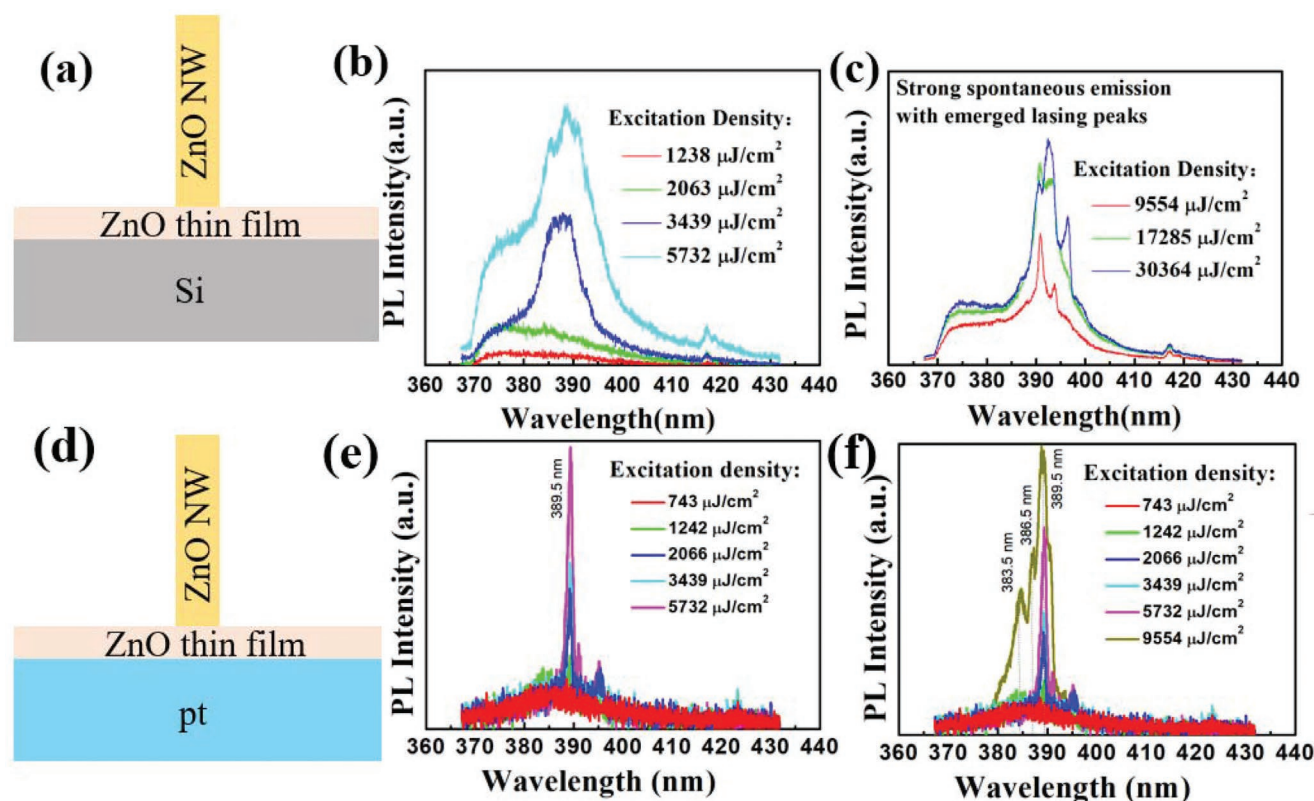
The room temperature PL spectra of the ZnO NWs with and without the Pt layer is shown in Figure 3a,b, for the ZnO NWs supported with Pt metal, an enhanced and broaden UV emission peak around 378 nm with the FWHM of 16 nm is observed, this emission peak could be attributed to near band edge emission.<sup>[42,43]</sup> Meanwhile, another very weak defects-related emission band located at around 550 nm could also be observed, this emission in ZnO is generally considered being originated from oxygen vacancies.<sup>[44]</sup> It could be noted that applying Pt metal under the end facet of NWs, resulted in improving the band edge emission, and thus enhancing

the overall PL emission (the ratio of peak intensity  $[I_{\text{with Pt}}/I_{\text{without Pt}}]$  is 170%) followed by broaden emission spectra width ( $\text{FWHM}_{\text{with Pt}}/\text{FWHM}_{\text{without Pt}} = 1.45$ ) in the UV region. Meanwhile, the relative UV to visible emission is dramatically enhanced ( $\text{UV/Vis}_{(\text{without Pt})} = 85$ ,  $\text{UV/Vis}_{(\text{with Pt})} = 240$ ) for ZnO NWs with Pt layer, it is concluded that the ratio of UV to defect luminescence depends on interface properties and crystal quality of the active media. Here, UV luminescence dominates the emission spectra for the ZnO NWs sample. In order to explore the mechanisms of UV emission in ZnO NWs supported with Pt layer, temperature-dependent PL spectra have been carried out in the temperature range from 88–312 K as shown in Figure 4c, which demonstrates bound exciton (BE) dominated emission accompanied with phonon coupled  $E_v$  peak (it is generally considered that the  $E_v$  peak was regarded as a free-to-bound [FB] transition).<sup>[26,43]</sup> Meanwhile, analytical fitting demonstrates a nonlinear correlation between photon energy and temperature (Figure 4d), which follows exponential decay mode as shown in the formula, it was observed that a clear transition from bandgap emission (3.371 eV) to BE emission occurs when gradually increasing the temperature from low to room temperature.

### 2.4. Optical Stimulated Emission Characterization of ZnO NWs without and with Pt Metal

The optical stimulated emission devices are composed of vertically aligned ZnO NWs without and with Pt as shown in





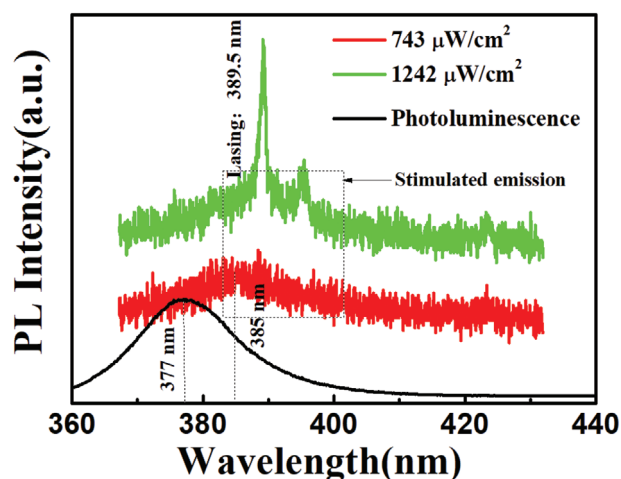
**Figure 4.** Ultraviolet lasing characterization of ZnO NWs without and with Pt metal at room temperature. a) Schematic configuration of ZnO NW photonic device, the circularly polarized excitation laser with focused beam over the ZnO NWs. The emission light was collected from the top facet of the NWs. b) Spontaneous emission of photonic laser device below the threshold at room temperature with varied excitation energy density. Mini emerged F-P lasing peaks located at the shoulder of the main spectra. c) Excitation energy density-dependent emission of the ZnO NW photonic device. Several sharp peaks emerged around 390 nm appears above the spontaneous band-edge emission background. d) Schematic configuration of ZnO NW/thin-film/Pt metal device, e) spontaneous emission of laser device under low excitation density. f) High excitation density-dependent emission of the ZnO NW/thin-film/Pt metal device. Clearly sharp emission peaks with preferentially single laser mode at around 390 nm appear with weak spontaneous emission background.

Figure 3a,d, which are optically pumped by 355 nm using an optical parametric amplifier (OPA) in an active-passive mode-locked femtosecond Ti: sapphire laser under the temperature of 20 °C (Figures S1 and S2, Supporting Information). It could be observed that F–P oscillations over band-edge emission of ZnO occurred, which demonstrates the resonated cavity modes could be observed in the longitudinal direction between end facets. To explore photonic mode lasers, the excitation power density-dependent emission spectra for ZnO NWs on Si substrate are shown in Figure 3b,c. At low excitation energy density below the threshold of 743, 1242  $\mu\text{J cm}^{-2}$ , the spectra are comprised of spontaneous emission located at  $\approx 375$  nm (Figure 3b), which could be attributed to band edge transition.<sup>[45]</sup> Dominant emission peaks located at  $\approx 388$  nm emerged with further increasing excitation densities (2066, 3439  $\mu\text{J cm}^{-2}$ ), this emission is 150 meV below the bandgap, which is generally ascribed to the recombination of excitons through an exciton-exciton collision process, where one of the excitons recombines to generate a photon corresponding to amplified spontaneous emission.<sup>[46]</sup> When the energy density further exceeds this value (5732  $\mu\text{J cm}^{-2}$ ), at the lower energy side of the broad spontaneous emission band, several mini sharp emission peaks emerged, the linewidth of these sharp peaks is much smaller

than that of the spontaneous emission peak, which could be clearly observed when further increasing excitation density to 9554  $\mu\text{J cm}^{-2}$ . And the observed mode spacing is  $\approx 3$  nm for  $\approx 3 \mu\text{m}$  long NWs (Figure 3c), which agrees quantitatively well with the calculated interspacing between adjacent resonance frequencies.<sup>[17]</sup>

$$\nu_F = c/2nl \quad (1)$$

where  $\nu_F$  is emission mode spacing,  $c$  is the speed of light,  $n$  is the refractive index, and  $l$  is the resonance cavity length. The cavity length could be calculated as  $\approx 3 \mu\text{m}$ . For the ZnO NW supported with Pt metal, the stimulated emission was as shown in Figure 3d, and a lower lasing threshold could be realized, which is 7.69 times smaller than that for the ZnO NW/thin+film/Si device with single emission mode at around 390 nm, through excitation density-dependent emission measurement, largely suppressed spontaneous emission could be clearly observed (Figure 3e,f), and 170% increased Q-factor from 411 to 700 was realized at the wavelength of  $\approx 390$  nm ( $Q = \lambda/\Delta\lambda$ , where  $\lambda/\Delta\lambda$  represent the peak wavelength and its FWHM) laser emission, the FWHM value of the mode was below 0.003 eV. As shown in Figure S3, Supporting Information,



**Figure 5.** PL spectra of the ZnO NW/thin-film/Pt metal sample under different excitation conditions for comparison, the evolution of the emission properties changes from PL emission at 377 nm to lasing emission at 389.5 nm could be clearly captured.

the integrated intensity ( $I$ ) of the emission peaks increases super linearly versus the excitation power density (IEX). And a transition from the spontaneous emission to lasing at  $1242 \mu\text{J cm}^{-2}$  could be observed. Narrow line-width, clear emission modes, and threshold indicate that the lasing emission has occurred in the ZnO NWs. It is observed that the emission intensity of the single lasing mode preferentially amplifies with larger excitation from  $1242$  to  $5732 \mu\text{J cm}^{-2}$ . When a larger excitation density of  $9554 \mu\text{J cm}^{-2}$  was applied for the ZnO NW/thin-film/Pt sample, more lasing modes emerged at the shoulder of the dominant lasing mode at  $\approx 390$  nm, which demonstrates that multi-lasing modes still exist in the NW F-P cavities when the stimulating power is high enough to survive corresponding emission modes. However, laser mode selectivity of the designed cavity length of  $3 \mu\text{m}$  allows preferential amplification of single-mode at around  $390$  nm. To repeat the optically stimulated emission, another ZnO NW/thin-film/Pt metal sample under excitation-dependent conditions was also carried out as shown in Figure S4, Supporting Information, it could be observed that clearly sharp emission peaks with the lasing mode at  $389.5$  nm. As the excitation density changes from  $743$  to  $9554 \mu\text{J cm}^{-2}$ , more lasing modes could also be observed under a higher excitation density, accompanied by weak spontaneous emission background, which agrees well with the experimental results observed in advance. Through interface integration of ZnO NWs with Pt metal, strong light confinement was thus realized to make lasing emission with a high internal gain. To clearly show the evolution of the emission changes of the ZnO NW/thin-film/Pt sample, spontaneous

to lasing emission trend could be clearly captured as shown in Figure 5.

## 2.5. Lasing Analysis of ZnO NWs without and with Pt Metal

Obviously, strong light confinement is achieved for lasing emissions through interface engineering by applying ZnO NWs with Pt metal. For excitation density larger than the threshold, the spectra are dominated by sharp emission peaks, the intensities of which are greatly larger than those for spontaneous emission background. Through non-linear fitting of laser mode intensity with excitation energy density for ZnO NW/thin-film/Pt metal sample, for example,  $I_{\text{KZ}} \sim I_{\text{ex}}^n$ , where the obtained  $n$  here equals  $1.46$  (Figure S3, Supporting Information), which illustrates rapid amplification for the realized laser mode.<sup>[47,48]</sup> To realize the optically pumped lasing emission, the laser cavity is a definitive character for lasers. Since the refractive index of ZnO ( $2.45$ ) is larger than that of air ( $1.0$ ) and Pt ( $1.68$  at  $390$  nm), the well-faceted top and bottom surfaces of the ZnO NW serve as mirrors that define an optical microcavity. The threshold gain  $G_{\text{th}}$  of the NW laser could be expressed as the following equation:

$$g_{\text{th}} = \alpha + \frac{1}{2L} \ln \frac{1}{R_1 R_2} \quad (2)$$

where  $\alpha$  is the loss along the length,  $L$  is the NW length, and  $R$  is the end facet reflection. According to this formula, the threshold gain is a strong function of the length and the facet reflection. For a given cavity length, the high reflectivity would lead to enhancement of the internal gain, and meanwhile, reduce the threshold for lasing. The measured reflectivity for Si assisted with Pt layer is much higher than that for only Si substrate in the whole spectra range from  $2.0$  to  $3.4$  eV. The reflectivity for Si is  $45.5\%$  with the photon energy of  $3.10$  eV, while that for Pt thin layer/Si substrate is  $69.3\%$ . (Figure S5, Supporting Information) Thus, the enhanced spontaneous and laser emissions could be achieved based on ZnO NWs through efficient interface light confinement, resulting in improved laser output performance by NW end facet engineering, which gives direct proof for constructing advanced nanosized optoelectronic devices.

As shown in Table 1, through analysis of lasing emissions for ZnO NWs without and with Pt metal it could be clearly observed that emission modes with mode interspacing of  $\approx 3$  nm, lower laser threshold could be achieved considering its enhanced internal gain when the excitation density is larger than the threshold, preferentially single lasing mode at around  $390$  nm with suppressed spontaneous emission dominant the transition process, which could be amplified when increasing

**Table 1.** Lasing parameters (including threshold, lasing mode, mode spacing, Q factor and single mode) analysis of ZnO NWs with and without Pt metal samples for comparison.

Samples	Threshold [ $\mu\text{J cm}^{-2}$ ]	Lasing modes [nm]	Mode spacing [nm]	Q factor	Single mode (preferential)
ZnO NWs without Pt	9554	— 387 390 393 396	$\approx 3$	411	No
ZnO NWs with Pt	1242	383.5 386.5 389.5 392.5 —	$\approx 3$	700	Yes

excitation density. However, more lasing modes still exist when excitation density is high enough ( $9554\mu\text{J cm}^{-2}$ ). Compared with the parameters for ZnO NWs without Pt sample, it could be observed that amplified stimulated emissions dominate the whole transition process under varying different excitation densities. Through strong light confinement for obtaining sufficient gain, ZnO NWs lasers could be well optimized to realize lasing emissions with a low light loss.<sup>[49,50]</sup>

### 3. Conclusion

In conclusion, strong light confinement was realized by applying ZnO NWs through interface engineering end facet by introducing Pt metal, a fully integrated NW laser device with cavity facet interface engineering was constructed, and optimized UV spontaneous and lasing emission was realized by reducing inner light loss from F-P cavities to substrate, supporting an effective optical path through interface engineering for photon extraction. 170% PL emission enhancement was realized, and a lower laser threshold could be achieved when the Q factor becomes high enough. And more lasing modes still exist when excitation density is high enough with lasing emission modes interspacing of around 3 nm. It is believed that performance improved optical devices could be realized by light-matter interaction tailoring, and advanced light emission devices such as LEDs and lasers could be constructed considering surface/interface engineering, which supplies a solution for improving optoelectronic device performances, especially in nanoscience and nanotechnology fields.

### 4. Experimental Section

**Preparation of Vertically Aligned ZnO NWs without and with Pt Metal:** Firstly, Pt thin films (thickness: 300 nm) were deposited on Si (100) substrates by a radio-frequency (RF) magnetron sputtering method using a 99.999% pure Pt target under a power of 130 W, respectively. Before being loaded into the sputtering chamber, the Si substrates were cleaned with organic solvents and rinsed with deionized water to remove the contamination. During the sputtering process, only argon gas with a flow rate of 30 standard cubic centimeters per min (SCCM) was used. Secondly, a thin layer of ZnO (with a thickness of  $\approx 30$  nm) was sputtered on the Pt thin films serving as a seed layer. The growth pressure for the sputtering ZnO layer was maintained at 1 Pa using mixed gases of oxygen and argon with a flow rate of 20 SCCM. The substrates were kept at room temperature (RT) with a rotation speed of 20 loops per min. Thirdly, the patterned area was realized by applying UV photolithography, and a partial bare ZnO seed layer was applied for ZnO NWs synthesis. Finally, a hydrothermal method was used to grow ZnO NWs using  $\text{Zn}(\text{CH}_3\text{COO})_2 \cdot 2\text{H}_2\text{O}$  and  $\text{C}_6\text{H}_{12}\text{N}_4$  as reactant sources. The reaction solution was adjusted to an identical concentration ( $0.01\text{ mol L}^{-1}$ ), and the surface of the ZnO seed layers was loaded towards the bottom of the reaction kettle. The reaction kettle was put into an oven and maintained at  $90^\circ\text{C}$  for 16 h. The obtained samples were rinsed with deionized water and dried in the oven.

**Characterization of ZnO NWs with Apparatus Applied:** The morphology of the samples was investigated by a field-emission SEM (FESEM: Hitachi S4800 microscope) equipped with an energy-dispersive X-ray (EDX). The crystal structure of the sample was studied by a Bruker D8GADDS XRD using Cu KR radiation. The PL measurement was performed using a JY-630 micro-Raman spectrometer with the 325 nm line of He-Cd laser as an excitation source. A mode-locked femtosecond Ti: sapphire laser with an OPA was employed for the stimulated

emission measurement of the ZnO NW samples, and the spectrum recorder (2300i spectrometer) was composed of nitrogen-cooled charge-coupled device (CCD) detector.

### Supporting Information

Supporting Information is available from the Wiley Online Library or from the author.

### Acknowledgements

This work was supported by National Key R&D Program of China (No. 2021YFB32012), National Natural Science Foundation of China (No.61874133, No.61901469, No.22005331), Key Research and Development Program of Jiangsu Province (No.BE2018080, No.BE2019684, No.BE2020768), Jihua Laboratory Foundation (No.X190181TD190), Youth Innovation Promotion Association CAS (No.2019322, No.2018360, No.Y201856), Instrument Developing Project of the Chinese Academy of Sciences (No.YJKYYQ20190057, No.YJKYYQ20200046, No. ZDKYYQ20210004), Science and Technology Development Program of Suzhou (No.SYG201907), Basic Research Pilot Project of Suzou (No. SJC2021019).

### Conflict of Interest

The authors declare no conflict of interest.

### Data Availability Statement

The data that support the findings of this study are available from the corresponding author upon reasonable request.

### Keywords

interface engineering, light confinement, ultraviolet lasing, ZnO nanowires

Received: January 5, 2022

Revised: March 26, 2022

Published online: June 1, 2022

- [1] Y. J. Lu, J. Kim, H. Y. Chen, C. H. Wu, N. Dabidian, C. E. Sanders, C. Y. Wang, M. Y. Lu, B. H. Li, X. G. Qiu, W. H. Chang, L. J. Chen, G. Shvets, C. K. Shih, S. Gwo, *Science* **2012**, 337, 450.
- [2] A. A. Toropov, E. A. Evropeitsev, M. O. Nestoklon, D. S. Smirnov, T. V. Shubina, V. K. Kaibyshev, G. V. Budkin, V. N. Jmerik, D. V. Nechaev, S. Rouvimov, S. V. Ivanov, B. Gil, *Nano Lett.* **2020**, 20, 158.
- [3] Z. Huang, Z. Zhong, H. Wang, S. Lu, J. Wang, G. Liu, T. Wei, J. Yan, J. H. Min, W. L. Jeong, D. S. Lee, X. Cai, F. Xu, X. Chen, D. Cai, J. Wang, J. Kang, *J. Phys. Chem. Lett.* **2020**, 11, 2559.
- [4] K. C. Shen, C. T. Ku, C. Hsieh, H. C. Kuo, Y. J. Cheng, D. P. Tsai, *Adv. Mater.* **2018**, 30, 1706918.
- [5] Y. Lee, D. Yoon, S. Yu, H. Sim, Y. Park, Y. S. Nam, K. J. Kim, S. Y. Choi, Y. Kang, J. Son, *Adv. Mater.* **2021**, 34, 2107650.
- [6] B. Xie, R. J. Wong, T. H. Tan, M. Higham, E. K. Gibson, D. Decarolis, J. Callison, K. F. Aguey-Zinsou, M. Bowker, C. R. A. Catlow, J. Scott, R. Amal, *Nat. Commun.* **2020**, 11, 1615.

- [7] S. Liu, W. Luo, D. Li, Y. Yuan, W. Tong, J. Kang, Y. Wang, D. Li, X. Rong, T. Wang, Z. Chen, Y. Li, H. Wang, W. Wang, J. Hoo, L. Yan, S. Guo, B. Shen, Z. Cong, X. Wang, *Adv. Funct. Mater.* **2020**, *8*, 2008452.
- [8] H. Ci, H. Chang, R. Wang, T. Wei, Y. Wang, Z. Chen, Y. Sun, Z. Dou, Z. Liu, J. Li, P. Gao, Z. Liu, *Adv. Mater.* **2019**, *31*, 1901624.
- [9] W. Khan, P. P. Potts, S. Lehmann, C. Thelander, K. A. Dick, P. Samuelsson, V. F. Maisi, *Nat. Commun.* **2021**, *12*, 5130.
- [10] L. Li, K. Wang, H. Fan, X. Zhu, J. Mu, H. Yu, Q. Zhang, Y. Li, C. Hou, H. Wang, *Mater. Horiz.* **2021**, *8*, 1711.
- [11] Y. Sun, X. Xie, Y. Chen, B. Sun, C. Wang, *ACS Nano* **2019**, *13*, 772.
- [12] M. B. Muhlestein, C. F. Sieck, P. S. Wilson, M. R. Haberman, *Nat. Commun.* **2017**, *8*, 15625.
- [13] B. Mayer, A. Regler, S. Sterzl, T. Stettner, G. Koblmüller, M. Kaniber, B. Lingnau, K. Ludge, J. J. Finley, *Nat. Commun.* **2017**, *8*, 15521.
- [14] D. Jevtics, A. Hurtado, B. Guilhabert, J. McPhillimy, G. Cantarella, Q. Gao, H. H. Tan, C. Jagadish, M. J. Strain, M. D. Dawson, *Nano Lett.* **2017**, *17*, 5990.
- [15] D. Saxena, F. Wang, Q. Gao, S. Mokkaapati, H. H. Tan, C. Jagadish, *Nano Lett.* **2015**, *15*, 5342.
- [16] S. Mokkaapati, D. Saxena, Nian-Jiang, Q. Gao, H. H. Tan, C. Jagadish, in *IEEE Int. Semiconductor Laser Conf. 2014*, IEEE, Palma de Mallorca, Spain **2014**, 217.
- [17] Y. G. Ma, X. Guo, X. Q. Wu, L. Dai, L. M. Tong, *Adv. Opt. Photonics* **2013**, *5*, 216.
- [18] S. Ullah, S. Pian, F. Dai, Y. Wang, Y. Ma, Q. Yang, *Front. Chem.* **2020**, *8*, 631870.
- [19] V. Saadattalab, A. Shakeri, H. Gholami, *Prog. Nat. Sci.: Mater. Int.* **2016**, *26*, 517.
- [20] M. M. Tavakoli, H. T. Dastjerdi, J. Zhao, K. E. Shulenberger, C. Carbonera, R. Po, A. Cominetti, G. Bianchi, N. D. Klein, M. G. Bawendi, S. Gradecak, J. Kong, *Small* **2019**, *15*, 1900508.
- [21] F. Lin, X. Liao, C. P. Liu, Z. S. Zhang, S. Liu, D. Yu, Z. M. Liao, *ACS Omega* **2020**, *5*, 4133.
- [22] J. Lu, C. Xu, F. Li, Z. Yang, Y. Peng, X. Li, M. Que, C. Pan, Z. L. Wang, *ACS Nano* **2018**, *12*, 11899.
- [23] X. X. Wang, C. X. Xu, F. F. Qin, Y. J. Liu, A. G. Manohari, D. T. You, W. Liu, F. Chen, Z. L. Shi, Q. N. Cui, *Nanoscale* **2018**, *10*, 17852.
- [24] K. Sarkar, S. Mukherjee, G. Wiederrecht, R. D. Schaller, D. J. Gosztola, M. A. Strosio, M. Dutta, *Nanotechnology* **2018**, *29*, 095701.
- [25] M. Wille, C. Sturm, T. Michalsky, R. Roder, C. Ronning, R. Schmidt-Grund, M. Grundmann, *Nanotechnology* **2016**, *27*, 225702.
- [26] J. Theerthagiri, S. Salla, R. A. Senthil, P. Nithyadharseni, A. Madankumar, P. Arunachalam, T. Maiyalagan, H. S. Kim, *Nanotechnology* **2019**, *30*, 392001.
- [27] V. Consonni, J. Briscoe, E. Karber, X. Li, T. Cossuet, *Nanotechnology* **2019**, *30*, 362001.
- [28] W. Liang, V. S. Ilchenko, D. Eliyahu, A. A. Savchenkov, A. B. Matsko, D. Seidel, L. Maleki, *Nat. Commun.* **2015**, *6*, 7371.
- [29] M. Yuan, W. Wang, X. Wang, Y. Wang, Q. Yang, D. Cheng, Y. Liu, L. Huang, M. Zhang, B. Liang, W. Zhao, W. Zhang, *Opt. Lett.* **2021**, *46*, 4855.
- [30] A. K. Tagantsev, S. A. Fedorov, *Phys. Rev. Lett.* **2019**, *123*, 043602.
- [31] Y. Zhang, C. Fowler, J. Liang, B. Azhar, M. Y. Shalaginov, S. Deckoff-Jones, S. An, J. B. Chou, C. M. Roberts, V. Liberman, M. Kang, C. Rios, K. A. Richardson, C. Rivero-Baleine, T. Gu, H. Zhang, J. Hu, *Nat. Nanotechnol.* **2021**, *16*, 661.
- [32] J. H. Kim, H. S. Lee, G. H. An, J. Lee, H. M. Oh, J. Choi, Y. H. Lee, *ACS Nano* **2020**, *14*, 11985.
- [33] L. Sortino, P. G. Zotev, S. Mignuzzi, J. Cambiasso, D. Schmidt, A. Genco, M. Assmann, M. Bayer, S. A. Maier, R. Sapienza, A. I. Tartakovskii, *Nat. Commun.* **2019**, *10*, 5119.
- [34] Y. Ashida, A. Imamoglu, E. Demler, *Phys. Rev. Lett.* **2021**, *126*, 153603.
- [35] M. Mirhosseini, E. Kim, X. Zhang, A. Sipahigil, P. B. Dieterle, A. J. Keller, A. Asenjo-Garcia, D. E. Chang, O. Painter, *Nature* **2019**, *569*, 692.
- [36] D. Zhao, W. Liu, G. B. Zhu, Y. Y. Zhang, Y. C. Wang, W. Y. Zhou, C. X. Xu, S. S. Xie, B. S. Zou, *Nano Energy* **2020**, *78*, 105339.
- [37] L. Tang, J. Qiu, Q. Wei, H. Gu, B. Du, H. Du, W. Hui, Y. Xia, Y. Chen, W. Huang, *ACS Appl. Mater. Interfaces* **2019**, *11*, 29132.
- [38] J. P. Prieto-Ruiz, S. G. Miralles, H. Prima-Garcia, A. Lopez-Munoz, A. Riminucci, P. Graziosi, M. Aeschlimann, M. Cinchetti, V. A. Dediu, E. Coronado, *Adv. Mater.* **2019**, *31*, 1806817.
- [39] P. Du, J. Li, L. Wang, L. Sun, X. Wang, X. Xu, L. Yang, J. Pang, W. Liang, J. Luo, Y. Ma, J. Tang, *Nat. Commun.* **2021**, *12*, 4751.
- [40] M. Y. Li, K. Shen, H. Xu, A. Ren, J. Lee, S. Kunwar, S. Liu, J. Wu, *Small* **2020**, *16*, 2004234.
- [41] T. Kinoshita, T. Matsuda, T. Takahashi, M. Ichimiya, M. Ashida, Y. Furukawa, M. Nakayama, H. Ishihara, *Phys. Rev. Lett.* **2019**, *122*, 157401.
- [42] Y. Wu, Y. Dai, S. Jiang, C. Ma, Y. Lin, D. Du, Y. Wu, H. Ding, Q. Zhang, N. Pan, X. Wang, *Phys. Chem. Chem. Phys.* **2017**, *19*, 9537.
- [43] B. R. Huang, J. P. Chu, C. L. Hsu, Y. S. Chen, C. H. Chang, *ACS Appl. Mater. Interfaces* **2017**, *9*, 39475.
- [44] J. Rodrigues, S. Medeiros, P. M. Vilarinho, M. E. V. Costa, T. Monteiro, *Phys. Chem. Chem. Phys.* **2020**, *22*, 8572.
- [45] A. Singh, K. Senapati, B. Satpati, P. K. Sahoo, *Phys. Chem. Chem. Phys.* **2017**, *21*, 14012.
- [46] K. Zidek, K. B. Zheng, M. Abdellah, N. Lenngren, Chabera, T. Pullerits, *Nano Lett.* **2012**, *12*, 6393.
- [47] B. Chon, J. Truong, M. Hansen, J. I. Hahm, Y. J. Lee, *ACS Photonics* **2019**, *6*, 1416.
- [48] S. Geburt, M. Lorke, A. L. da Rosa, T. Frauenheim, R. Roder, T. Voss, U. Kaiser, W. Heimbrod, C. Ronning, *Nano Lett.* **2014**, *14*, 4523.
- [49] X. Zhang, R. Yi, N. Gagrani, Z. Li, F. Zhang, X. Gan, X. Yao, X. Yuan, N. Wang, J. Zhao, P. Chen, W. Lu, L. Fu, H. H. Tan, C. Jagadish, *ACS Nano* **2021**, *15*, 9126.
- [50] F. Zhang, X. Zhang, Z. Y. Li, R. Yi, Z. Li, N. Wang, X. Xu, Z. Azimi, L. Li, M. Lysevych, X. Gan, Y. Lu, H. H. Tan, C. Jagadish, L. Fu, *Adv. Funct. Mater.* **2022**, *32*, 2103057.